2023 5th International Conference on Control Systems, Mathematical Modeling, Automation and Energy Efficiency (SUMMA) | 979-8-3503-0912-6/23/$31.00 ©2023 IEEE | DOI: 10.1109/SUMMA60232.2023.10349667

Mathematical Modelling of a 0.68/0.75 μm Optical Filter Based on Photonic Crystal Fibre and Au Surface Plasmon Resonance

Younis Mohamed Atiah
dept. Physics
College of Education, University of Misan
Maysan, Iraq
ORCID:0000-0003-2861-6643

Imad H. Agha
dept. Physics
University of Dayton
Dayton, USA
ihagha@gmail.com

Ahmed M. Zheoat
dept. Pharmacy
Al-Manara, College for Medical Sciences, Misan
Maysan, Iraq
ORCID:0000-0002-8353-6235

A. Shchegolkov
Department of Technology and Methods of Nanoproducts Manufacturing, Tambov State Technical University
Tambov, Russian Federation
Energynano@yandex.ru

Murtadha M. Al-Zahiwat
dept. Petroleum Engineering
University of Misan, College of Engineering
Maysan, Iraq
ORCID:0000-0002-8526-8668

***Abstract*—The filter is designed with air holes distributed in a hexagonal shape, and in the core of the filter, there are four gold rods to achieve surface plasmon resonance (SPR). The effect of the air hole's diameter and the hole-pitch (p) dimension on the effective mode area (X-polarization) and the Confinement Loss was studied using the finite element method (FEM). This analysis found evidence that the hole-pitch (p) is the most crucial factor that affects confinement loss value without shifting the resonant wavelength. In addition, increasing the air hole's diameter (d) can affect the amount of power transferred by changing the refractive index and shifting the resonant wavelength toward longer wavelengths. Our results demonstrated that could attain a maximum confinement loss of 332.95 dB⁄cm and a minimum effective mode area of 10.44 μm² for p=1.9 μm and d= 1.2 μm at λ=0.75 μm. The control d (1.2, 1.3, 1.4, and 1.6) μm can be used to produce different induced resonant wavelengths (0.68, 0.7, 0.72, and 0.75) μm respectively. This filter has a lot of advantages, like being able to filter out wavelengths between 0.68 and 0.75 μm, and it can be used for a bunch of different things in biotech and medicine. Additionally, PCF has a simple structure and is simple to manufacture.**

Keywords—Photonic crystal, Surface plasmon resonance, Optical filter

I. INTRODUCTION

Photonic crystal fiber (PCF), also known as "holey fiber," this type of fiber has tiny, cylinder air holes spaced at regular intervals along its entire length [1]. Photonic-Bandgap guiding occurs when the optical fibers holes distribution is changed to improve optical fiber performance. For example, PCF can be changed as follows: elliptical holes distribution [2], octagonal holes distribution [3], square holes distribution [4], and hexagonal holes distribution [5]. The PCF was used in a pharmacy to test pharmaceutical items containing vitamins B (B1), B6, B12, and C from various suppliers [6], as well as, the refractive features of PCF have been applied to bacteria [7] , COVID [8] and cancer detection [9]in the field of sensors.

In modern optical communications, using photonic crystals, they can control light rays in the near-infrared. This can help improve optical systems by increasing light transmission and light direction [10]. PCF filters provide a great degree of design freedom and may eliminate undesired wavelengths caused by noise. There are various solutions to this problem in the literature. Khaleque and Hattori, for example, investigated an optical filter with an elliptical metal film at 1310 nm and a loss of 1221 dB/cm for the direction x polarized [11]. Wang et al. suggested a gold nanofilm optical filter with a loss of 8578 dB/cm at the resonant wavelength of 1310 nm [12]. Yang et al. used a silver-filled liquid-filled silver sheet to create a polarization filter at 1550 nm with a loss of 305 dB/cm [13]. Dan Yang have reported a D-shaped filter based on Surface Plasmon Resonance (SPR) with a loss 1307.90dB/cm at 1310 nm [14]. Several filters in the wavelength range (0.68-0.75) μm are utilized for a variety of applications. In high-content screening [15] and DNA sequencing [16], for example, optical filters (0.68 μm) can eliminate undesirable background fluorescence noise. Furthermore, in molecular technology, optical filters can minimize excitation light noise or scattered light from the excitation source [17]. Furthermore, optical filters improve two-photon deep tissue imaging in the (0.68-0.75) μm range [18]. Another form of filter known as a "Barrier filter" is used in biotechnology and biomedicine to avoid unwanted excitation light in the fluorescence emission area (0.68 μm) [19]. Providing a quick and easy technique to identify vegetation and measure the general health of plants in the field of agriculture [20]. One of the main objectives of this paper was to design a four- layer hexagonal air hole optical filter with SPR, this filter operates in the (0.68 - 0.75) μm range. The filter's performance can be improved by adjusting the air hole diameter (d) and hole pitch (p). Meanwhile, this design can be used in place of other filters whose efficiency is uncontrollable.

II. PROPOSED PCF APPROACH

Transmission and coupling properties of PCFs were studied for performance analysis with the help of COMSOL commercial software integrated with FEM solvers and combined with PML (Perfect Match Layer) in COMSOL software 5.2

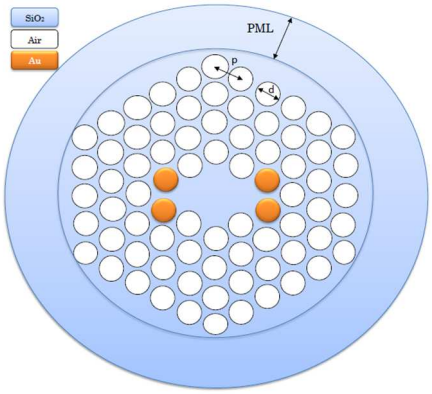

Fig. 1. Cross section details of PCF

A PCF filter diagram via SPR with four gold rods is shown in Figure (1). PML is a layer that is 14.3 µm. The gold rod is the orange circle. The mode near the core of the PCF was computed using the FEM. Using Sellmeier's equation and the values of (1) provided in Table (1), it is possible to estimate how the refractive index of SiO_2 varies with wavelength [21].

$$n(\lambda) = \sqrt{1 + \frac{A_1\lambda^2}{\lambda^2-\lambda_1} + \frac{A_2\lambda^2}{\lambda^2-\lambda_2} + \frac{A_3\lambda^2}{\lambda^2-\lambda_3}} \quad (1)$$

TABLE I. PARAMETERS OF SELLMEIER'S EQUATION

A1	*A2*	*A3*
0.6961663	0.4079426	0.8974794
λ_1 µm²	**λ_2 µm²**	**λ_3 µm²**
0.0684043	0.1162414	9.896161

Drude-Lorentz model for metal was used to calculate the relative permittivity of gold as [22]. Table 2 shows the parameters of (2), where ω=2πc/λ, c is speed of light.

$$\varepsilon_{Ag} = \varepsilon_\infty - \frac{\omega_D^2}{\omega(\omega - j\gamma_D)} - \frac{\Delta\varepsilon\,\Omega_L^2}{(\omega^2-\Omega_L^2) - j\Gamma_L\,\omega} \quad (2)$$

TABLE II. PARAMETERS OF RELATIVE PERMITTIVITY FOR GOLD

ε_∞	$\gamma_D/2\pi$ (THz)	$\omega_D/2\pi$ (THz)	$\Omega/2\pi$ (THz)	$\Gamma_L/2\pi$ (THz)	$\Delta\varepsilon$
5.967	15.92	2113.6	650.07	104.86	1.09

The effective mode area is calculated as: [23]

$$A_{eff} = \frac{\iint_{-\infty}^{\infty}|F(x,y)|^2dxdy}{\iint_{-\infty}^{\infty}|F(x,y)|^4dxdy}, \quad (3)$$

The incident and surface plasmon resonance modes are treated dependently, The SPR effect is based on coupled mode theory is given by the following equations: [24]

$$\frac{dE_{inc}}{dz} = i\kappa_1 E_{inc} + iC_{12}E_{SPR}, \quad (4)$$

$$\frac{dE_{SPR}}{dz} = iC_{21}E_{inc} + i\kappa_2 E_{SPR}, \quad (5)$$

C_{21}, C_{12} are coupling coefficient between the E_{inc} and E_{SPR} modes and n is refractive index of the SiO_2.

κ_1 , κ_2 are the propagation constants of the E_{inc} and E_{SPR} of electric field of core and SPR modes respectively, and given by:

$$\kappa_1 = \sqrt{\varepsilon_{SiO_2}}\kappa_0 \;, \kappa_2 = n\kappa_0\sqrt{1 - \left(\frac{|\varepsilon_{SiO_2}|}{|\varepsilon_{Ag}|}\right)} \quad (6)$$

where ε_{SiO_2} is permittivity of SiO_2. The general solution of (4 and 5) can be written in matrix form as:

$$\frac{d}{dz}\begin{bmatrix}E_{inc}\\E_{SPR}\end{bmatrix} = i\begin{bmatrix}\kappa_1 & C_{12}\\C_{21} & \kappa_2\end{bmatrix}\begin{bmatrix}E_{inc}\\E_{SPR}\end{bmatrix} \quad (7)$$

The eigenvalue of κ can be found by applying the following equation:

$$\frac{d}{dz}\begin{bmatrix}E_{inc}\\E_{SPR}\end{bmatrix} = \begin{bmatrix}E_{inc}\\E_{SPR}\end{bmatrix}e^{i\kappa z} \quad (8)$$

From (7), let matrix transformation $\mu = \begin{bmatrix}\kappa_1 & C_{12}\\C_{21} & \kappa_2\end{bmatrix}$ and the determinant of a matrix of (7 and 8) given by:

$$det|\mu - \kappa I| = 0, \quad (9)$$

I is the identity matrix (9) can be used to find κ.

$$(\kappa_1 - \kappa)(\kappa_2 - \kappa) - C_{12}C_{21} = 0, \quad (10)$$

Since the center of the PCF is symmetric, then $C_{12} = C_{21} = C$, κ satisfies the quadratic equation given by:

$$\kappa_\pm = (\kappa_1 + \kappa_2/2) \pm \gamma\,, \quad (11)$$

where $\gamma = \sqrt{(\kappa_1 - \kappa_2/2) + C^2}$, The coupling coefficient, which governs the PCF coupling between the E_{inc} and E_{SPR}, is given by: [25]

$$C = \frac{\kappa_0\iint_{-\infty}^{\infty}\delta n|F(x,y)|^2dxdy}{\iint_{-\infty}^{\infty}|F(x,y)|^2dxdy}, \quad (12)$$

If the mode is homogenous, the coupling coefficient is given by:

$$C = 2\pi\delta n/\lambda, \quad (13)$$

The refractive index (Δn) based on p for SiO_2 is obtained by a Fourier series of periodic index variations within the center of the PCF is given by: [26]

$$\Delta n = \sum_{m=-\infty}^{\infty} n\,e^{-\frac{2\pi imz}{p}}, \quad (14)$$

The real part of the refractive index of SiO_2 is given by:

$$\Delta n = n\cos\left(\frac{2\pi}{p}z\right), \quad (15)$$

The complex refractive index δn in (12) that results is the sum of the contributions of p and the wavelength.

$$\delta n = \Delta n + n(\lambda), \quad (16)$$

The confinement loss (CL) can be calculated by using the following equation: [27]

$$\alpha(\lambda) = 8.686 \times \mathrm{Im}[\delta n)] \times \kappa_0 \times 10^4(\mathrm{dB/cm}), \quad (17)$$

Im[δn] is the complex refractive index (imaginary part) and $\kappa_0 = 2\pi/\lambda$, when κ_1=κ_2, κ in (11) is given by:

$$\kappa_{\pm} = \kappa_1 \pm (2\pi/\lambda)\delta n, \quad (18)$$

By using the boundary condition that E_{inc} is incident on the core such that $E_{inc} = E_{inc}(0)$ and $E_{SPR} = 0$, the solution of (4 and 5) is given by:

$$E_{inc}(z) = E_{inc}(0)[\cos \gamma z + i(\kappa_1 - \kappa_2/2\gamma)\sin(\gamma z)], \quad (19)$$

$$E_{SPR}(z) = E_{SPR}(0)(iC/\gamma)\sin(\gamma z), \quad (20)$$

III. Results and Discussion

The electric field distributions of one of the PCF's modes are depicted in Figure 2.

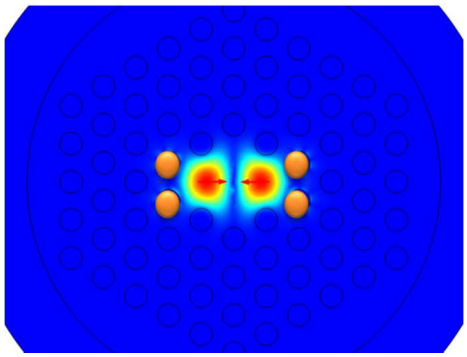

Fig. 2. Electric field distributions of the core mode

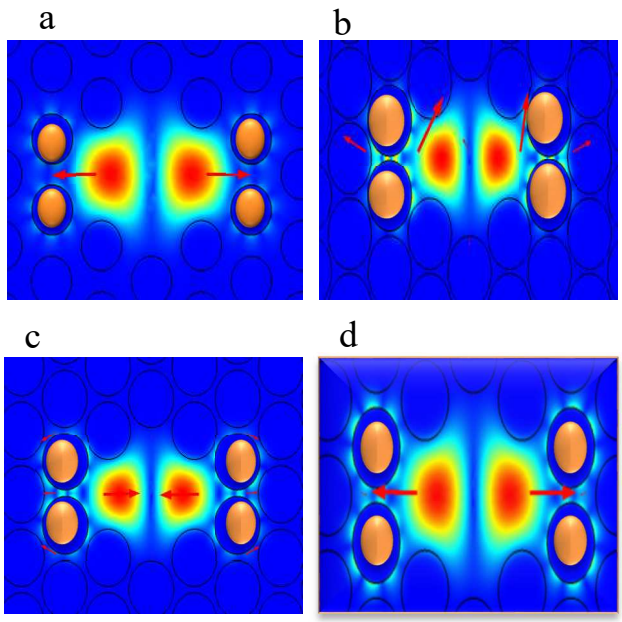

Fig. 3. Modal field distribution (a) core mode (X-polarization) (b)at λ=0.72 μm and (c) at λ=0.74 μm the beginning of SPR modes generation around a surface the gold rods (d) SPR modal field at λ=0.75 μm .

The core mode is shown in Figure 3(a). The distribution of the core mode and the start of plasmon phenomena surrounding the surface of gold rods are shown in Figures 3 (b) and (c). The resonant coupling between the SPR and the core mode is shown in Figure 3(d). Figure 4 depicts the effective index of the core mode (blue line) and SPR mode (green curve) as a function of wavelength, as well as CL spectrum of the core mode (red curve). Note that the resonance wavelengths 0.68 μm and 0.75 μm happen when the line of the effective index of the core mode intersects with the line of effective index SPR mode at Re[neff] = 1.4376 (SPR1) and, Re[neff] = 1.4399 (SPR2). When incident light strikes the interface between SiO_2, air, and the surface of the rods gold, setting κ_1-κ_2=0, C= γ, and using (19 and 20), the following equations are obtained:

$$P_{inc}(z) = P_{inc}(0)\cos^2(\gamma z)\ , \quad (21)$$

$$P_{SPR}(z) = P_{SPR}(0)\sin^2(\gamma z), \quad (22)$$

where $P_{inc} = |E_{inc}|^2$ is incident power and $P_{SPR} = |E_{SPR}|^2$ is plasmon power.

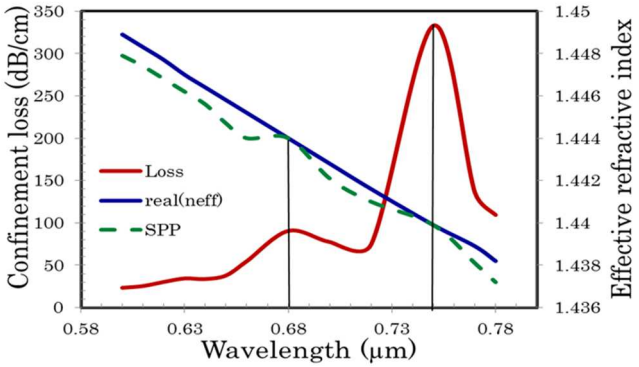

Fig. 4. Real part of the Re[neff](Blue curve), the SPR mode (Green curve), and the confinement loss spectrum (Red curve).

A. *The Effect of the (d) on the Effective Mode Area(X-polarization).*

Figure 5 indicates the Effective Mode Area (EMA) varying with wavelength. Two EMA of SPR1 and SPR2 are observed at the wavelengths of 0.68 μm (λ_{SPR1}) and 0.75 μm (λ_{SPR2}), based on SPR phenomena, it is deduced that fundamental mode interacts with SPR mode at 0.68 μm and 0.75 μm . EMA of the core modes reaches a maximum at 8 μm^2 for the resonant wavelength 0.68 μm and 10.1 μm^2 for the resonant wavelength 0.75 μm.

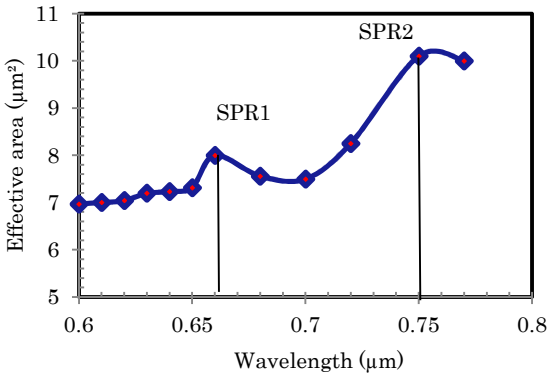

Fig. 5. EMA of core mode vs. wavelength

EMA curves for various d diameters are shown in Figure 6. As seen in Figure 6, the EMA of the core mode decreases as d increases. The explanation for this behavior might be due to the fact that the increase in d leads to a narrowing of the core, and the thickness of the air circumference around the core of the PCF increases, As a result, κ_1 and κ_2 vary depending on the boundary condition of the air/ SiO_2/ Au interface as shown in (6).

Another interesting observation is that the EMA at the resonant wavelength moves toward the longer wavelength

(red-shifted) with increasing (d), it is obvious that changing the d causes the varying of the phase matching in the core mode and induces a phase shift. It can be explained by A_{eff} is essentially related to the coupling coefficient $C=2\pi\delta n/\lambda$, it is quite clear that C of core mode is modulated by δn.

The resonance wavelengths are 0.68, 0.7, 0.72, and 0.75 µm and the corresponding EMAs are 10.1, 10.24, 10.3, and 10.5 µm^2 respectively, as shown in Figure 6.

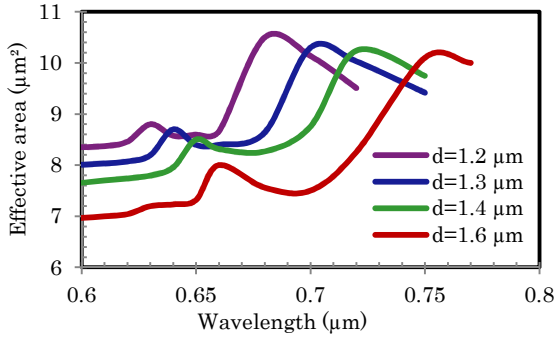

Fig. 6. EMA vs. wavelength for p=2.2 µm, d=1.2, 1.3, 1.4 and 1.6 µm

As shown in Figure 7, the (d) mostly influences the resonance wavelength. And it also has minimal effect on the EMA at SPR1 and SPR2.

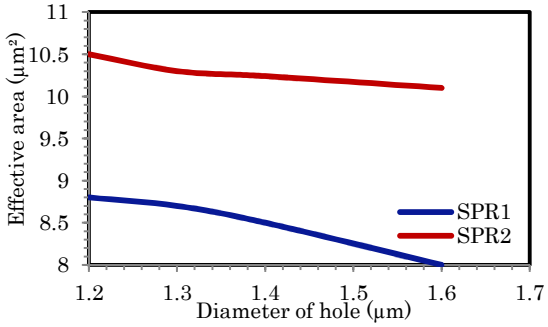

Fig. 7. EMA of core mode for p=2.2 µm , d=1.2, 1.3, 1.4 and 1.6 µm

B. *The Effect of the (p) on the Effective Mode Area(X-polarization).*

Figure 8 shows the effect of various (p) values on the EMA for the core mode, first point, the curves of EMA are exactly identical; second point, there is no shift in the peaks of SPR1 or SPR2 as a result of the influence of (p). It can also be noticed from Figure 8 the increase in EMA as a result of the increase in (p). This is because a larger (p) increases the SiO_2 of the core relative to the air holes. Additionally, it should be noted that the increase in(p) does not influence the resonance wavelength because (p) in this range (p = 1.9-2.3 µm), does not affect phase-matching condition.

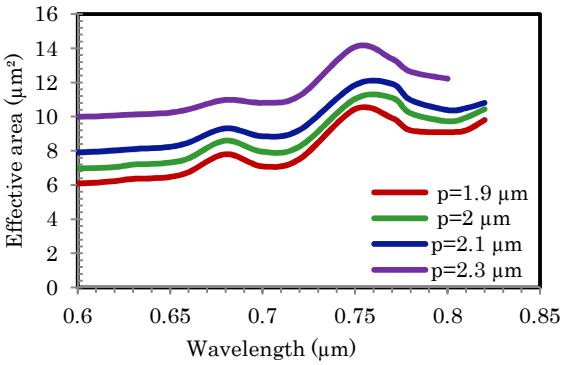

Fig. 8. EMA vs. wavelength for d=1.2 µm, p=1.9, 2, 2.1 and 2.3µm

For the hole-pitch p = 1.9, 2, 2.1, and 2.3 µm, the EMA of the SPR2 are 10.44, 11.04, 11.855, and 14.085 µm^2 and those of the SPR1 are 7.8, 8.6, 9.3, and 10.98 µm^2, respectively, as shown in Figure 9.

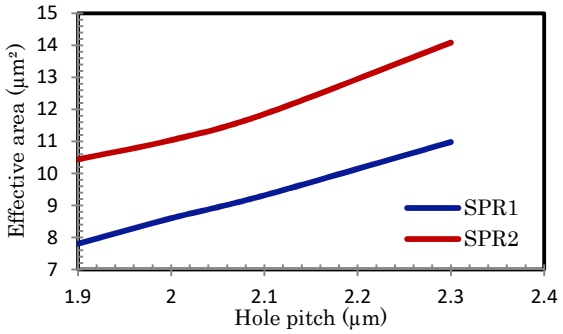

Fig. 9. EMA of core mode for d=1.2 µm, p=1.9, 2, 2.1 and 2.3µm

C. *The Effect of the (d) on the C L*

The CL was estimated by utilizing the imaginary part of the effective mode index according to (17). Figure10 indicates the CL spectrum in core mode, SPR1 (κ_-) and SPR2 (κ_+) are observed at the wavelengths of 0.68 µm and 0.75 µm. Figure 11 shows the CL of core mode when the(d) is selected as 1.2 µm, 1.3 µm, 1.4 µm, and 1.6 µm. It can be found that SPR resonant wavelengths red shift with an increase in (d) at the same (p). Meanwhile, the value of the CL is increasing with an increase in (d).

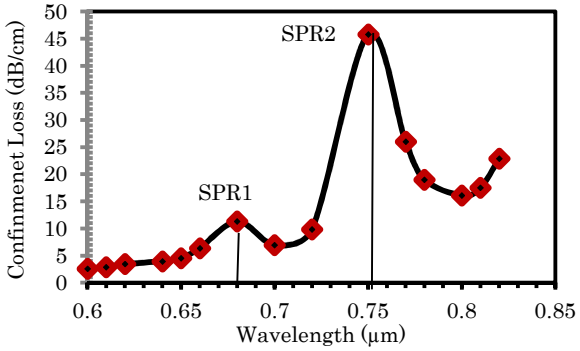

Fig. 10. CL vs. wavelength

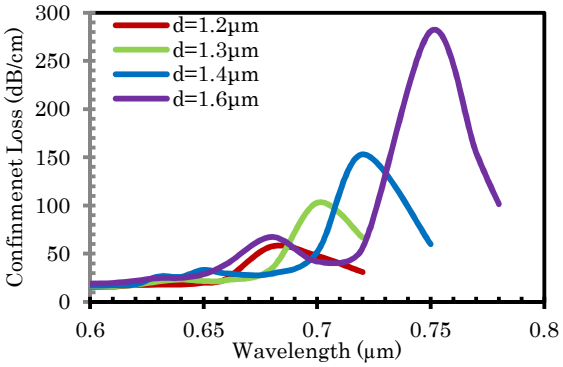

Fig. 11. C L vs. wavelength for p=2.2 µm ,d=1.2, 1.3, 1.4, and 1.6 µm

The result of CL in Figure 12 shows that when d = 1.2, 1.3, 1.4 and 1.6 µm, the CLs are 57.6, 102.9 , 153, and 280.7 dB/cm respectively. In addition, an increase in d = 1.2, 1.3, 1.4 and 1.6 µm leads to resonance wavelengths 0.68, 0.7, 0.72 and 0.75µm, respectively. Hence, the resonance wavelength value is easily controlled by changing the value of (d).

Note that the $\gamma = \sqrt{(\kappa_1 - \kappa_2/2) + C^2} = C = 2\pi\delta n/\lambda$,at $\kappa_1 = \kappa_2$ .An increase in d leads to an increase in the air in the holes which has a low refractive index compared to the material of the core (SiO_2), therefore the δn of the core mode is changing , A change in δn changes the coupling coefficient (C), which induces a phase shift. In addition, the $P_{SPR}(0)$ in $P_{SPR}(z) = P_{SPR}(0)\sin^2(\gamma z)$ is increased.

According to (21 and 22), If γz = (π /4), the $P_{inc}(0)$ is distributed equally between core mode and SPR mode; if γ z = (π/2), all of $P_{inc}(0)$ is transferred into SPR mode; and if γz = (π), all of their $P_{SPR}(0)$ is returned to core mode.

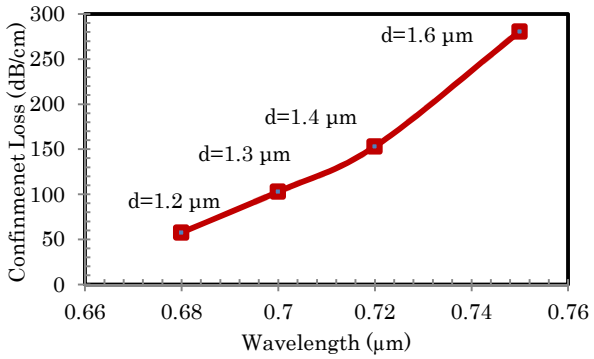

Fig. 12. CL vs. wavelength at d=1.2, 1.3, 1.4, and 1.6 µm

D. The Effect of the (p) on the CL

Figure 13 illustrates the CL of the core mode when p = 1.9, 2, 2.1, 2.2, and 2.3 µm. By fixing the (d) and changing the (p), it is noting that the value of SPR2 increases as (p) decreases, although the resonant wavelengths remain constant at 0.68 µm (SPR1) and 0.75 µm (SPR2). Furthermore, the behavior of the CL curve is same, and there is no shift in the resonant wavelengths as (p) increases. As a result, the (p) can control the amount of CL, while the resonance wavelength remains constant. This is because the reduction of (p) and fixed (d) in this PCF structure decreases the air in the holes and increases the material of the core (SiO_2), this indicates that (γz) in $P_{SPR}(z) = P_{SPR}(0)\sin^2(\gamma z)$ is still constant with an increase in (p).

At 0.75 µm resonance wavelength, the CL for p = 1.9, 2, 2.1, 2.2, and 2.3 µm are 332.95, 280.74, 240.73, 192.59, and 149.97 dB/cm, respectively. Moreover At 0.68 µm resonance wavelength the CL for p = 1.9, 2, 2.1, 2.2, and 2.3 µm are 90.55, 67.38, 45.88, 31.39, and 22.43 dB/cm, respectively.

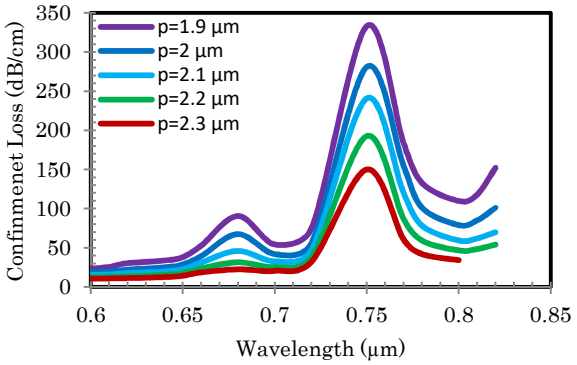

Fig. 13. CL vs. wavelength for d=1.2 µm ,p=1.9, 2, 2.1, 2.2 and 2.3µm

The main findings from the table.3 are as follows: 1. Maximum CL for Y-polarized core mode is observed in most of the studies (with the exception of Lu et al., 2018; Hossen, 2019), whereas our results indicate a high maximum CL for X-polarized core mode 2. The wavelengths of the resonance are 1.31 and 1.55 µm, while our results show that the wavelengths of the resonance are 0.68 and 0.75 µm.

TABLE III. COMPARISON RESULTS BETWEEN THE PROPOSED DESIGN FILTER AND THE OTHER DESIGNS FILTER.

Ref.	Resonance wavelength (µm)	CL (dB/cm)	SPR
[28]	1.31	508	Gold-layer
[29]	1.55	630.20	Gold-layer
[30]	1.31-1.55	234	Gold-layer
[31]	1.55	718.87	Gold-layer
[32]	1.55	1304.02	Gold film
[33]	1.31 - 1.55	234	Gold film
[34]	1.55	563.29	Gold film
[35]	1.55	1024.84	Gold film
[36]	1.31-1.55	251.26	Gold rod
[37]	1.42	692.25	Gold wires
[38]	1.519 - 1.664	573.33-543.21	Gold owire
[39]	1.2-1.3475 -1.567	946.63- 826.79- 737.13	Gold rod
[40]	0.75-0.85- 0.9 - 1	312.6- 438 - 376.8 - 285.2	Gold rod

IV. CONCLUSIONS

The SPR-based hexagonal photonic crystal filter has a basic design and is easy to fabricate. Gold is the metal used to create the plasmonic phenomena. A mathematical modelling technique and a mathematical model of plasmonic phenomena in the hexagonal photonic crystal filter have been developed. The finite element method was utilized to investigate the effective mode area and CL of the core mode, as well as the characteristics of the proposed PCF filter. According to the results, the resonance wavelengths of the proposed PCF filter are 0.68 µm, 0.7 µm, 0.72 µm, and 0.75 µm depending on (d). In addition, the amount of CLs can be adjusted by changing (p). When λ_{SPR} =0.75 µm and d=1.2 µm the following CLs are observed: (a) 332.95 dB⁄cm at p=1.9 µm (b) 280.74 dB⁄cm at p=2 µm (c) 240.73 dB⁄cm at p=2.1 µm (d) 192.59 dB at p=2.2 µm (e) 149.97 dB/cm at p=2.3 µm. Consequently, when λ_{SPR} =0.68 µm and d=1.2 µm(a) 90.55 dB⁄cm at p=1.9 µm (b) 67.38

dB⁄cm at p=2 μm (c) 45.88 dB⁄cm at p=2.1 μm (d) 31.39 dB at p=2.2 μm (e) 22.43 dB/cm at p=2.3 μm.

ACKNOWLEDGMENT

This work is made possible by the Ministry of Higher Education and Scientific Research/University of Misan Department of Physics, and Al-Manara, College for Medical Sciences,IRAQ,https://uomisan.edu.iq/en/, info@uomanara.edu.iq

REFERENCES

[1] Liu, Zihan, Jialin Wen, Zhengyong Zhou, Yuming Dong, and Tianyu Yang. "A Highly Birefringent Photonic Crystal Fiber with Three Rows of Circular Air Holes," *In Photonics*, vol. 10, no. 5, p. 527. MDPI, (2023).

[2] K R. Hao, Z. Li, G. Sun, L. Niu, and Y. Sun, "Analysis on photonic crystal fibers with circular air holes in elliptical configuration," *Optical Fiber Technology,* vol. 19, pp. 363-368, (2013).

[3] Hossain, Md Selim, Shuvo Sen, and Md Mahabub Hossain. "Performance analysis of octagonal photonic crystal fiber (O-PCF) for various communication applications," *Physica Scripta* 96, no. 5 055506, (2021).

[4] Tasolamprou, A. C., Kafesaki, M., Soukoulis, C. M., Economou, E. N., & Koschny, T. "Chiral topological surface states on a finite square photonic crystal bounded by air," *Physical Review Applied*, 16(4), 044011,(2021).

[5] Sen, S., Abdullah-Al-Shafi, M., & Kabir, M. A. "Hexagonal photonic crystal Fiber (H-PCF) based optical sensor with high relative sensitivity and low confinement loss for terahertz (THz) regime," *Sensing and Bio-Sensing Research*, 30,100377,(2020).

[6] Kumari, Anamika, Vibha Vyas, and Santosh Kumar "Advances in electrochemical and optical sensing techniques for vitamins detection: A review." *ISSS Journal of Micro and Smart Systems* 11, no.1,329-341, (2022).

[7] Suthar, Bhuvneshwer, and Anami Bhargava. "Enhanced optical sensor for waterborne bacteria-based photonic crystal using graded thickness index." *Applied Nanoscience* 1-8,(2023).

[8] Gupta, Ankur, Tanu Singh, Rajat Kumar Singh, and Akhilesh Tiwari. "Numerical Analysis of Coronavirus Detection Using Photonic Crystal Fibre–Based SPR Sensor." *Plasmonics* 18, no. 2 577-585, (2023):

[9] Abdelghaffar, M., Yusuf Gamal, Reda A. El-Khoribi, Wafaa Soliman, Y. Badr, Mohamed Farhat O. Hameed, and S. S. A. Obayya. "Highly sensitive V-shaped SPR PCF biosensor for cancer detection." *Optical and Quantum Electronics* 55, no. 5,472,(2023).

[10] Volk, Andrew, Amit Rai, Imad Agha, Jimmy E. Touma, Tamara Payne, and Rudra Gnawali. "Novel Photonic Crystals for Beam Control in the Near-Infrared Spectrum." In *2022 IEEE Research and Applications of Photonics in Defense Conference (RAPID)*, pp. 1-2. IEEE, (2022).

[11] A. Khaleque and H. T. Hattori, "Polarizer based upon a plasonic resonant thin layer on a squeezed photonic crystal fiber," *Appl. Opt.* 54(9), 2543–2549, (2015). **DOI: 10.1364/AO.54.002543**

[12] G. Y. Wang et al., "A kind of broadband polarization filter based on photonic crystal fiber with nanoscale gold film," *Plasmonics* 12(2), 377–382, (2017). **https://doi.org/10.1007/s11468-016-0274-6**

[13] X. Yang et al., "Design of a tunable single-polarization photonic crystal fiber filter with silver-coated and liquid-filled air holes," *IEEE Photonics* J. 9(4), 7105108,(2017).

[14] Yang, D., Li, Y., Xu, B., Wei, Z., Cheng, T., & Wang, X. Modified D-type surface plasmon resonance (SPR)-based photonic crystal fiber (PCF) for application as a polarization filter and refractive index sensor. *Instrumentation Science & Technology*, *51*(2), 162-182,(2023). **https://doi.org/10.1080/10739149.2022.2109161**

[15] Zaghmi, Ahlem, Erdem Aybay, Long Jiang, Mingmei Shang, Julia Steinmetz-Späh, Fredrik Wermeling, Per Kogner et al. "High-content screening of drug combinations of an mPGES-1 inhibitor in multicellular tumor spheroids leads to mechanistic insights into neuroblastoma chemoresistance." *Molecular Oncology* (2023).

[16] Bonet, David Fernandez, and Ian T. Hoffecker. "Image recovery from unknown network mechanisms for DNA sequencing-based microscopy." *Nanoscale* 15, no. 18 (2023): 8153-8157.

[17] Hüpfel, Manuel, Andrei Yu Kobitski, Weichun Zhang, and G. Ulrich Nienhaus. "Wavelet-based background and noise subtraction for fluorescence microscopy images." *Biomedical Optics Express* 12, no. 2 (2021): 969-980.

[18] Zhao, Zhifeng, Yiliang Zhou, Bo Liu, Jing He, Jiayin Zhao, Yeyi Cai, Jingtao Fan et al. "Two-photon synthetic aperture microscopy for minimally invasive fast 3D imaging of native subcellular behaviors in deep tissue." *Cell* 186, no. 11 (2023): 2475-2491.

[19] Jun, Seongmoon, Minho Choi, Baul Kim, Martina Morassi, Maria Tchernycheva, Hyun Gyu Song, Hwan-Seop Yeo, Noëlle Gogneau, and Yong-Hoon Cho. "Enhancement of Single-Photon Purity and Coherence of III-Nitride Quantum Dot with Polarization-Controlled Quasi-Resonant Excitation." *Small* 19, no. 5 2205229,(2023).

[20] Stamford, John D., Silvere Vialet-Chabrand, Iain Cameron, and Tracy Lawson. "Development of an accurate low cost NDVI imaging system for assessing plant health." *Plant Methods* 19, no. 1 9, (2023).

[21] Ji, Xingchen, Yoshitomo Okawachi, Andres Gil-Molina, Mateus Corato-Zanarella, Samantha Roberts, Alexander L. Gaeta, and Michal Lipson. "Ultra-Low-Loss Silicon Nitride Photonics Based on Deposited Films Compatible with Foundries." *Laser & Photonics Reviews* 17, no. 3, 2200544, (2023).

[22] Wang, Dongying, Yang Yu, Zhechun Lu, Junbo Yang, Zao Yi, Qiang Bian, Jianfa Zhang et al. "Design of photonic crystal fiber to excite surface plasmon resonance for highly sensitive magnetic field sensing." *Optics Express* 30, no. 16 (2022): 29271-29286.

[23] Fu, H., Liu, C., Yi, Z., Song, X., Li, X., Zeng, Y., Wang, J., Lv, J., Yang, L. and Chu, P.K., "A new technique to optimize the properties of photonic crystal fibers supporting transmission of multiple orbital angular momentum modes." *Journal of Optics*, *52*(1), pp.307-316,(2023) .

[24] Snyder, A.W.; Love, J.D. Optical Waveguide Theory; Chapman&Hall: London, UK, 1983; pp. 542–552.

[25] A. Yariv, *Optical Electronics in Modern Communications*, 5th ed. (Oxford University Press, New York, 1997).

[26] Matera, F., A. Mecozzi, M. Romagnoli, and M. Settembre. "Sideband instability induced by periodic power variation in long-distance fiber links." *Optics Letters* 18, no. 18 ,1499-1501, (1993).

[27] Amiri, I.S., Yupapin, P. and Rashed, A.N.Z., "Mathematical model analysis of dispersion and loss in photonic crystal fibers," *Journal of Optical Communications*, *44*(1), pp.139-144,(2023).

[28] Xue, J.R.; Li, S.G.; Xiao, Y.Z.; Qin, W.; Xin, X.J.; Zhu, X.P. Polarization filter characters of the gold-coated and the liquid filled photonic crystal fiber based on surface plasmon resonance. *Opt. Express*, 21, 13733–13740, (2013).

[29] C. Dou, X. L. Jing, S.G. Li, Q. Liu, J. A Bian, "Photonic Crystal Fiber Polarized Filter at 1.55μm based on Surface Plasmon Resonance," *Plasmonics*,vol.11,pp.1163-1168,(2016).

[30] Zhao, Y.; Li, S.; Liu, Q.; Wang, X. Design of a novel photonic crystal fiber filter based on gold-coated and elliptical air holes. *Opt. Mater.* 73, 638–641,(2017)

[31] Wang, Yujun, Shuguang Li, Hailiang Chen, Min Shi, and Yingchao Liu. "Ultra-wide bandwidth polarization filter based on gold-coated photonic crystal fiber around the wavelength of 1.55 μm." Optics & Laser Technology 106 , 22-28, (2023).

[32] Zhao, X.T.; Hua, L.; Jiang, G.H.; Cheng, J.R.; Xiong, Q. A "Novel Polarization Filter Based on Photonic Crystal Fiber with a Single Au-Coated Air Hole and Semi-Hourglass Structure." *Plasmonics*,14,1725–1733,(2019).

[33] Chen, Nan, Xuedian Zhang, Min Chang, Xinglian Lu, and Jun Zhou. "Broadband plasmonic polarization filter based on photonic crystal fiber with dual-ring gold layer." *Micromachines* 11, no. 5 470, (2020). **https://doi.org/10.3390/mi11050470**

[34] Zhang, Yongxia, Jinhui Yuan, Yuwei Qu, Xian Zhou, Binbin Yan, Qiang Wu, Kuiru Wang, Xinzhu Sang, Keping Long, and Chongxiu Yu. "Design of diamond-shape photonic crystal fiber polarization filter based on surface plasma resonance effect." *Chinese Physics B* 29, no. 3 ,034208, (2020). **DOI: 10.1088/1674-1056/ab683c**

[35] Wang, Chao, Guoxu Zhang, Zheng Wu, Yajing Zhang, Yiyang Zhang, Linghong Jiang, and Weihong Bi. "A broadband gold-coated photonic crystal fiber polarization filter with a high loss ratio of both polarizations at 1550 and 1310 nm." *In Photonics*, vol. 8, no. 11, p. 488. MDPI, (2021).
https://doi.org/10.3390/photonics8110488

[36] Lu, X.L.; Chang, M.; Chen, N.; Zhang, X.D.; Zhuang, S.L.; Xu, J. Design of a Metal-Filled Photonic-Crystal Fiber Polarization Filter Based on Surface Plasmon Resonance at 1.31 and 1.55 μm. *IEEE Photon. J*., 10, 7203913,(2018).

[37] M. N. Hossen, M. Ferdous, K. Ahmed, M. A. Khalek, S. J. Chakma, B.K. Paul, "Single polarization photonic crystal fiber filter based on surface plasmon resonance," *Front. Optoelectron*., vol.12, pp.157–164, (2019). **DOI: 10.1007/s12200-018-0843-8**

[38] Zhizhao Jin, Tao Lv, and Li Liu. "High extinction ratio and large bandwidth PCF polarization filter with gold-wires coated by monocrystalline silicon." *IEEE Photonics Journal* 14, no. 4, 1-6. (2022). **DOI: 10.1109/JPHOT.2022.3193395**

[39] Zhang, Shuanggen, Hui Zhou, Yangbo Bai, Lifang Xue, Bochi Guo, Wei Yan, Yu Liu, and Bin Li. "Design of a broadband dual-cladding PCF polarization filter via triple surface plasmon resonance effects." *Optics Communications* 546 129770,(2023). **https://doi.org/10.1016/j.optcom.2023.129770**

[40] Younis Mohamed Atiah,A.M Ghalambor Dezfuli and Hadeel Makki"The Study of SiO_2 and Ag plasmonic photonic crystal fiber for optical communication" *IEEE Conference (AICCIT-2023)*. **DOI: 10.1109/AICCIT57614.2023.10217996**